HHS Public Access

Author manuscript

Cancer Immunol Res. Author manuscript; available in PMC 2020 February 24.

Published in final edited form as:

Cancer Immunol Res. 2019 February ; 7(2): 244–256. doi:10.1158/2326-6066.CIR-18-0460.

Mouse PVRIG Has CD8+ T Cell–Specific Coinhibitory Functions and Dampens Antitumor Immunity

Benjamin Murter[#1], **Xiaoyu Pan**[#1], **Eran Ophir**[2], **Zoya Alteber**[2], **Meir Azulay**[2], **Rupashree Sen**[1], **Ofer Levy**[2], **Liat Dassa**[2], **Ilan Vaknin**[2], **Tal Fridman-Kfir**[2], **Ran Salomon**[2], **Achinoam Ravet**[2], **Ada Tam**[1], **Doron Levin**[2], **Yakir Vaknin**[2], **Evgeny Tatirovsky**[2], **Arthur Machlenkin**[2], **Drew Pardoll**[1], **Sudipto Ganguly**[1]

[1]Bloomberg–Kimmel Institute for Cancer Immunotherapy, Johns Hopkins University, Baltimore, Maryland. [2]Compugen Ltd, Holon, Israel.

[#] These authors contributed equally to this work.

Abstract

A limitation to antitumor immunity is the dysfunction of T cells in the tumor microenvironment, in part due to upregulation of coinhibitory receptors such as PD-1. Here, we describe that poliovirus receptor-related immunoglobulin domain protein (PVRIG) acts as a coinhibitory receptor in mice. Murine PVRIG interacted weakly with poliovirus receptor (PVR) but bound poliovirus receptor-like 2 (PVRL2) strongly, making the latter its principal ligand. As in humans, murine NK and NKT cells constitutively expressed PVRIG. However, when compared with humans, less PVRIG transcript and surface protein was detected in murine $CD8^+$ T cells *ex vivo*. However, activated $CD8^+$ T cells upregulated PVRIG expression. In the mouse tumor microenvironment, infiltrating $CD8^+$ T cells expressed PVRIG whereas its ligand, PVRL2, was detected predominantly on myeloid cells and tumor cells, mirroring the expression pattern in human tumors. PVRIG-deficient mouse $CD8^+$ T cells mounted a stronger antigen-specific effector response compared with wild-type $CD8^+$ T cells during acute *Listeria monocytogenes* infection. Furthermore, enhanced $CD8^+$ T-

Corresponding Author: Sudipto Ganguly, Johns Hopkins University School of Medicine and Sidney Kimmel Comprehensive Cancer Center, 1650 Orleans Street, CRB-1 Room 441, Baltimore, MD 21287. Phone: 410-614-2948; sgangul8@jhmi.edu.

Authors' Contributions

Conception and design: X. Pan, E. Ophir, Z. Alteber, O. Levy, L. Dassa, A. Machlenkin, D. Pardoll, S. Ganguly

Development of methodology: X. Pan, Z. Alteber, M. Azulay, I. Vaknin, D. Pardoll, S. Ganguly

Acquisition of data (provided animals, acquired and managed patients, provided facilities, etc.): X. Pan, Z. Alteber, M. Azulay, R. Sen, T. Fridman-Kfir, R. Salomon, A. Ravet, A. Tam, D. Levin, Y. Vaknin, E. Tatirovsky, S. Ganguly

Analysis and interpretation of data (e.g., statistical analysis, biostatistics, computational analysis): X. Pan, E. Ophir, M. Azulay, R. Sen, L. Dassa, T. Fridman-Kfir, R. Salomon, A. Ravet, D. Levin, Y. Vaknin, S. Ganguly

Writing, review, and/or revision of the manuscript: X. Pan, E. Ophir, Z. Alteber, L. Dassa, T. Fridman-Kfir, R. Salomon, A. Ravet, D. Levin, D. Pardoll, S. Ganguly

Administrative, technical, or material support (i.e., reporting or organizing data, constructing databases): B. Murter, X. Pan

Study supervision: X. Pan, E. Ophir, Z. Alteber, O. Levy, L. Dassa, I. Vaknin, A. Machlenkin, S. Ganguly

Note: Supplementary data for this article are available at Cancer Immunology Research Online (http://cancerimmunolres.aacrjournals.org/).

Disclosure of Potential Conflicts of Interest

D. Pardoll reports receiving commercial research funding from Bristol-Myers Squibb, Compugen, and Astra Zeneca; has ownership interest in Aduro Biotech, DNAtrix, Dracen, Ervaxx, Five Prime Therapeutics, Potenza, Tizona, Trieza, and WindMil; and is a consultant/advisory board member for Amgen, Bayer, DNAvax, FLX Bio, Immunomic, Janssen, Merck, Rock Springs Capitol, and Tizona. No potential conflicts of interest were disclosed by the other authors.

cell effector function inhibited tumor growth in PVRIG$^{-/-}$ mice compared with wild-type mice and PD-L1 blockade conferred a synergistic antitumor response in PVRIG$^{-/-}$ mice. Therapeutic intervention with antagonistic anti-PVRIG in combination with anti-PD-L1 reduced tumor growth. Taken together, our results suggest PVRIG is an inducible checkpoint receptor and that targeting PVRIG-PVRL2 interactions results in increased CD8^{+} T-cell function and reduced tumor growth.

Introduction

Tumor cells evade immune surveillance (1, 2). Cancer immunotherapies including immune-checkpoint blockade have been successful in the clinic, underscoring the value of the immune system in surveillance and elimination of cancer (3). Immune-checkpoint curtailment of T-cell effector functions is mediated by receptor-ligand axes such as CTLA-4-CD80/CD86 or PD-1-PD-L1/PD-L2. Monoclonal antibodies blocking immune-checkpoint pathways have been or are being developed that rescue dormant antitumor T-cell effector responses. Ipilimumab, a monoclonal antibody (Ab) that binds to CTLA-4, has been effective against melanoma (4). Antibodies that block PD-1 binding to its ligand, PD-L1, reduce tumor progression in more than 10 different cancer types (5, 6). However, single-agent immune-checkpoint inhibition does not cause remission in most cancer patients and, despite frequent durable remissions in responders, acquired resistance often develops (7). The identification and validation of additional immune-checkpoint inhibitors that can work alone or in combination remains a priority.

Among the immune-checkpoint pathways, a group of receptors and ligands within the nectin and nectin-like family are under intense investigation. Receptors within this family include DNAM-1 (CD226), CD96 (TACTILE), TIGIT, and PVRIG (CD112R; refs. 8–10). Of these molecules, DNAM is a costimulatory receptor that binds to two ligands, PVR (CD155) and PVRL2 (CD112; ref. 11). In contrast to DNAM-1, two inhibitory receptors in this family, TIGIT and PVRIG, have been shown to dampen human lymphocyte function (12, 13). TIGIT is reported to have a high-affinity interaction with PVR, a weaker affinity for PVRL2 and PVRL3, and inhibits both T-cell and NK cell responses through signaling of its intracellular tail or by inhibition of PVR-DNAM interactions to prevent DNAM signaling (14, 15). PVRIG binds only to PVRL2 with high affinity and suppresses T-cell function (10, 16). The affinities of TIGIT for PVR and PVRIG for PVRL2, respectively, are higher than the affinity of DNAM to either of its ligands. Collectively, these data indicate that there are three mechanisms by which TIGIT or PVRIG can suppress T-cell function: (i) direct inhibitory signaling through inhibitory motifs contained within their intracellular domains; (ii) sequestration of ligand binding from DNAM-1; and (iii) disruption of DNAM homodimerization and signaling. Within this family, PVR is also a ligand for CD96, whose immunomodulatory role on lymphocytes is less clear (17, 18). On the basis of these data, we postulated that within this family, there are two parallel inhibitory pathways, TIGIT binding to PVR and PVRIG binding to PVRL2, that could dampen T-cell function.

Although PVRIG functions as a human T-cell inhibitory receptor (10), the role of PVRIG and its ligand, PVRL2, in T cell-mediated cancer immunity has not been reported. Functional characterization of the mouse *Pvrig* gene and the effects stemming from

disruption of PVRIG-PVRL2 interaction *in vivo* in preclinical tumor models have also not been reported. In this study, we investigated the role of mouse PVRIG in syngeneic tumor models using PVRIG-knockout mice and anti-PVRIG. We demonstrate that PVRIG has a different expression profile on murine T-cell subsets compared with TIGIT and that its dominant ligand, PVRL2, is upregulated on myeloid and tumor cells in the tumor microenvironment (TME). Furthermore, inhibition of PVRIG-PVRL2 interaction reduced tumor growth in a $CD8^+$ T cell-dependent manner or with synergistic effects when combined with PD-L1 blockade. Collectively, these data show that mouse PVRIG is an inhibitory receptor that regulates T-cell antitumor responses.

Materials and Methods

Animals

Six-to-8-week-old C57BL/6 mice (Ozgene Pty Ltd) and BALB/c female mice (Envigo) were maintained in a specific pathogen-free (SPF) animal facility. $PVRIG^{-/-}$ mice were generated at Ozgene Pty Ltd and maintained in an SPF animal facility. C57BL/6 mice from Ozgene served as wild-type controls in all experiments. All studies were approved by the Institutional Animal Care and Use Committees at Johns Hopkins University (Baltimore, Maryland, USA) and Tel Aviv University (Tel Aviv, Israel).

Characterization of mouse PVRIG binding interactions

mPVRIG Fc (GenScript) and mPVRL2-his (R&D Systems, 3869-N2) were used for binding studies. For surface plasmon resonance (SPR) experiments, proteins were diluted to 100 nmol/L in acetate buffer pH 4.0 and were covalently coupled to a unique flow cell of a CM5 Series S Biacore chip (GE Healthcare Life Sciences) using standard amine coupling chemistry. Surfaces were activated with 1-ethyl-3-(3-dimethyl aminopropyl) carbodiimide; NHS = N-hydroxysuccinimide (EDC-NHS) and later blocked by injection of 1 mol/L ethanolamine (pH 8.5). Running buffer was 10 mmol/L Hepes pH 7.3, 150 mmol/L NaCl, 3 mmol/L EDTA, and 0.05% Tween-20 (HBS-EP+). Final immobilization amounts were ~ 1,000 RU. Proteins used as analytes were diluted to 2.5, 0.5, and 0.1 μmol/L. In each run, one tube contained running buffer for reference. After each run, a regeneration step with 4 mol/L MgCl2 for 30 seconds at 20 μL/sec was performed. For ELISA experiments, recombinant mouse PVRL2 HIS protein (Sino Biological) was diluted to 2 μg/mL and coated onto an EIA/RIA plate (Costar) overnight at 4°C. Coated plate wells were washed twice and incubated with blocking buffer at room temperature (RT) for 1 hour. After washing, plate-bound mPVRL2 was incubated with the recombinant receptor proteins: mouse PVRIG Fc, mouse DNAM-1 Fc (R&D Systems), mouse TIGIT Fc (R&D Systems), or an irrelevant isotype control Ab, at RT for 1 hour. A dose titration of the receptors (0–200 nmol/L) was performed. Plates were washed, and bound proteins were detected with horseradish peroxidase (HRP)-conjugated goat anti-mouse IgG secondary Ab was added. Data were analyzed using GraphPad Prism software.

For binding to B16F10 cells, mPVRIG Fc or mouse IgG2a protein (Bio X Cell) in serial dilution (0.1–3.2 μg/mL) was incubated with B16F10 cells for 40 minutes at RT. Cells were washed with FACS buffer, and bound proteins were detected by Goat Anti Mouse IgG2a-PE

(Jackson ImmunoResearch) for 20 minutes at RT. For knockdown experiments, B16-F10 cells were transfected using mouse PVRL2 siRNA pool (Dharmacon) or mouse PVR (Dharmacon) by Lipofectamine RNAiMAX Transfection Reagent (Invitrogen, cat. #13778–075) according to the manufacturer's procedure. Scrambled siRNA (Dharmacon) was used as a nontarget negative control. No modulation of PVRL2 expression by PVR siRNA or PVR expression by PVRL2 siRNA was observed. Binding of mPVRIG Fc to siRNA transfected cell was performed as described above.

Generation and characterization of anti-mouse PVRIG antibodiesc

cDNA encoding amino acids 22–152 for mouse PVRIG was cloned into expression plasmids (Aldevron GmbH). Groups of laboratory rats (Wistar) were immunized by intradermal application of DNA-coated gold particles using a hand-held device for particle-bombardment ("gene gun"). Serum samples were collected after a series of immunizations and tested in flow cytometry on HEK cells transiently transfected with the mPVRIG expression plasmids. Ab-producing cells were isolated and fused with mouse myeloma cells (Ag8) according to standard procedures. Hybridomas producing antibodies specific for PVRIG were identified by screening in the same assay as described above. Cell pellets of positive hybridoma cells were prepared using an RNA protection agent (RNAlater, Thermo Fisher Scientific) and further processed for sequencing of the variable domains of the antibodies. Anti-mouse PVRIG antibodies (0.1–10 μg/mL) were characterized by binding to HEK293 mouse PVRIG-overexpressing cells, or HEK293 empty vector control cells or D10.G4.1 endogenously express mouse PVRIG. Rat IgG2b-k Isotype control (BioLegend) at the same concentrations was used as a control. Goat anti-Rat PE-conjugated Ab (Jackson ImmunoResearch) was used for detection. Knockdown of PVRIG on D10.G4.1 was performed using siRNA (Dharmacon). For assessing PVRIG-PVRL2 antagonistic activity, anti-mouse PVRIG monoclonal Ab (clone 407) was tested for inhibiting mouse PVRL2 Fc binding to HEK293 mPVRIG cells and for inhibiting mouse PVRIG Fc fusion protein binding to B16F10 cells. For the mPVRIG Fc/B16F10 assay, 6.25 μg/mL mPVRIG Fc was preincubated with serial dilutions of anti-mPVRIG Abs or isotype control Ab for 30 minutes at RT before being added to B16F10 cells and incubated for an additional 40 minutes at RT. Cell-bound mPVRIG Fc was detected with Goat Anti-Mouse IgG2a-PE after 20-minute incubation at RT. For the PVRL2Fc/HEK293 mPVRIG assay, HEK293 mPVRIG cells were preincubated with anti-mPVRIG Ab and PVRL2 Fc added. Bound PVRL2 Fc was detected by Goat Anti-Mouse IgG2a-PE.

PVRIG expression profiling studies

RNA extraction was performed with the RNAeasy Mini Kit (Qiagen; cat. #74014) according to the manufacturer's protocol. cDNA was produced using the High-Capacity cDNA Reverse Transcription Kit (Applied Biosystems; cat. #4368814) following the manufacturer's instructions. cDNA was used as a template for qRT-PCR reactions, using a gene-specific TaqMan probe (Life Technologies; cat. #CC70L8H, CC6RN19 Custom). Detection was performed using QuantStudio 12k device. The cycle in which the reactions achieved a threshold level of fluorescence (Ct = threshold cycle) was registered and was used to calculate the relative transcript quantity in the RT reactions by using the equation Q

$= 2^{-Ct}$. The resulting relative quantities were normalized to the relative quantity of the housekeeping gene mRPL19 (Life Technologies; cat. # Mm02601633_g1).

For protein expression by flow cytometry, single-cell suspensions were stained with viability dye (Zombie NIR viability dye; BioLegend), and dead cells were excluded. To minimize nonspecific Ab binding, cells were preincubated with anti-CD16/CD32 (eBioscience) and 2% rat serum (STEMCELL Technologies) before staining with Abs specific to PVRIG, CD4, CD8, CD3, NK1.1, CD49b, or relevant isotype controls (BioLegend). All data were collected on a BD FACSCelesta flow cytometer (BD Biosciences) and analyzed with FlowJo software. For expression studies in tumor-bearing mice, mice were sacrificed 14 to 17 days after tumor implantation, and tumors, inguinal tumor-draining lymph node, and spleens were removed and processed. For tumors, single-cell suspensions were prepared by using the mouse Tumor Dissociation Kit and the gentleMACS Dissociator (Miltenyi Biotec) as per the manufacturer's protocol. For activation of T cells, $CD3^+$ cells were isolated from fresh splenocytes using the EasySep Mouse T-Cell Isolation Kit (STEMCELL Technologies) and were activated with anti-CD3/anti-CD28 beads (Gibco) at a 3:1 T cell:bead ratio along with 30 U/mL of recombinant human IL2 (BioLegend). Following activation of 11 days, cells were collected and studied for RNA and protein expression.

Mouse *in vitro* T-cell assays

Splenocytes from wild-type or $PVRIG^{-/-}$ mice were rested overnight. On the following day, cells were labeled with Cell Proliferation Dye eFluor450 (eBioscience) according to the manufacturer's instructions. Cells were plated in 24-well tissue culture plates precoated with 0.5 μg/mL anti-mouse CD3 (eBioscience, clone 145–2c11). Soluble PVRL2-Fc (GenScript) or control protein mIgG2a-Fc (Bio X Cell) at 10 μg/mL were added to the wells. T-cell proliferation was assessed by proliferation dye dilution on day 4.

Pmel-1 TCR transgenic mice possess $CD8^+$ T cells that specifically recognize a 25–33 amino acid epitope presented by $H2\text{-}D^b$ MHC class I molecules. Splenocytes were isolated from 8-to 10-week-old Pmel-1 TCR transgenic mice on either a $PVRIG^{-/-}$ or wild-type background and stimulated with 1 μg/mL of $mgp100_{25–33}$ (KVPRNQDWL, GenScript) and 50 U/mL recombinant human IL2 for 10 days. On the 10th day, $CD8^+$ T cells were isolated using a negative selection kit (Miltenyi) and cultured overnight with full medium supplemented with 50 U/mL of recombinant human IL2. On the following day, $CD8^+$ T cells and B16-F10/mhgp100 target cells (B16-F10 melanoma cells transduced with pMSGV1 retrovirus encoding a chimeric mouse gp100-human $gp100_{25–33}$ sequence; kindly provided by Dr. Ken-ichi Hanada, Surgery Branch, NCI) were cocultured at 2:1 E:T (5×10^4 T cells and 2.5×10^4 target cells) in 96-well round-bottom cell culture plates at 37°C, 5% CO_2 for 18 hours. Subsequently, cells were harvested and studied for expression of activation markers. In addition, culture supernatants were collected and assessed for cytokine secretion by a Mouse Th1/Th2/Th17 Cytometric Bead Array (BD).

Flow cytometry

Dissociated cells from tumors and lymphoid organs were filtered through a 100-μm filter and subjected to ACK buffer lysis of erythrocytes prior to FACS staining. Antibodies listed

in Supplementary Table S1 were used for staining immune and non-immune cell populations at pretitrated concentrations.

Cells (1×10^6) were seeded into a 96-well U-bottomed plate for staining. Samples were first stained with a viability dye (Live Dead Aqua; Thermo Scientific) in PBS, washed and resuspended in FACS buffer (FB; PBS containing 0.1% BSA and 2 mmol/L EDTA) with a cocktail of antibodies against CD16, CD32, and CD64 (BD Biosciences) to block nonspecific binding to all three Fc receptors. Samples were washed with FB and surface-stained with an isotype control or a target Ab cocktail. Samples were washed and acquired on a BD Fortessa flow cytometer. Analysis was done using BD FACSDiva.

Listeria monocytogenes Ova immunization

The double-attenuated strain of recombinant Ova-expressing *Listeria monocytogenes* (LmOva; deleted for actA and inlB; generously provided by Professor Jonathan Powell, Johns Hopkins University) was used in this study. Age- and gender-matched wild-type and PVRIG$^{-/-}$ mice were immunized (i.v.) with 10^6 CFU of LmOva. To assess primary LmOva-specific responses, spleens were harvested from immunized and nonimmunized mice on day 7 after infection. In additional experiments, wild-type and PVRIG$^{-/-}$ mice that had received primary immunization as above were challenged with a secondary immunization (10^7 CFU) on day 60, and spleens and bone marrow were harvested on day 67. Splenocytes (both time points) and bone marrow cells (day 67) were restimulated with 0.1 μg/mL $Ova_{257–264}$ peptide or $Ova_{323–339}$ peptide for 4 hours before intracellular cytokine staining and flow-cytometric analysis. To assess the accumulation of antigen-specific CD8$^+$ T cells following LmOva immunization on day 7, splenocytes from immunized and nonimmunized wild-type and PVRIG$^{-/-}$ mice were stained with a SIINFEKL H-2K^b tetramer. Because some H-2K^b tetramers have a tendency to stain all CD8$^+$ T cells by virtue of an interaction between CD8 and the α3 domain of the MHC molecule (19), we used a viable CD3$^+$ CD4$^-$ gate to collect data on CD8$^+$ T cells.

In vivo tumor models

A total of 5×10^5 (CT26 or MC38 colon carcinoma) or 2×10^5 (B16-F10 melanoma) cells were inoculated subcutaneously into the right flank of age-matched female mice. Ab treatment was initiated on day 4 (monotherapy dosing in CT26), day 7 (combination dosing in CT26), day 14 or day 25 (MC38) after tumor implantation. Abs were administrated intraperitoneally (i.p.) twice per week for 2 (MC38) or 3 (CT26) weeks. Tumor growth was measured with electronic caliper every 2 to 3 days and was reported as $0.5 \times W^2 \times L$ mm^3 (L is the length and W is the width of the tumor). Animals reaching 2,250 mm^3 (Tel Aviv University) or 5,000 mm^3 (Johns Hopkins University) tumor size were anesthetized. For studies done in the MC38 model, isotype controls (rat IgG2b; clone LTF-2; Bio X Cell) and anti-mouse PD-L1 (clone 10F.9G2; Bio X Cell) were dosed at 5 mg/kg. In CD8 depletion studies, anti-mouse CD8β (clone 53–5.8) and isotype control (rat IgG1; clone TNP6A7) were administered (5 mg/kg) on the day before, the day of implantation, and weekly thereafter. For studies done in the CT26 model, anti-mouse PD-L1 (clone YW243.55.S70; Compugen) and corresponding isotype control were dosed at 5 mg/kg, whereas a 10 mg/kg dose was used for rat IgG2b isotype control and anti-mouse PVRIG (clone 407). Statistical

analyses were performed using two-way ANOVA with repeated measures, followed by two-way ANOVA with repeated measures for selected pairs of groups using JUMP (Statistical Discoveries) software. Analyses of tumor growth measurements were performed by comparing tumor volumes measured on the last day on which all study animals were alive. Statistical differences in percentage of mice tumor free were determined by a log-rank Mantel-Cox test. Values of $P < 0.05$ were considered significant. *, $P < 0.05$; **, $P < 0.01$; ***, $P < 0.001$.

In vivo immune monitoring studies

In separate experiments, MC38 tumors were implanted into PVRIG$^{-/-}$ and wild-type mice as described above on day 0. Anti-mouse PD-L1 and isotype control antibodies were administered as above on days 14 and 17. On day 18, tumors, tumor-draining lymph nodes, and spleens were harvested from the four experimental groups. Spleens and tumors were processed into single-cell suspensions on a gentleMACS tissue dissociator (Miltenyi Biotec) using the mouse spleen and tumor dissociation kits (Miltenyi Biotec), respectively, following the manufacturer's instructions. Tumor suspensions were enriched for immune cells using mouse tumor-infiltrating lymphocyte (TIL) (CD45) microbeads (Miltenyi Biotec) and automatically separated into CD45$^+$ and CD45$^-$ fractions on the autoMACS Pro system (Miltenyi Biotec). Spleen suspensions were subjected to RBC lysis using ACK buffer before counting and flow-cytometric analysis. Tumor-draining and nondraining lymph nodes were dissociated over a 70-μm cell strainer using sterile 3 mL. syringe plungers and repeated flushing with ice-cold cell isolation medium (RPMI-1640 + 5% HIFCS + 2 mmol/L EDTA) prior to counting and flow cytometry.

Intracellular cytokine staining.—CD45$^+$ fractions from tumors along with spleen, tumor-draining, and nondraining lymph node suspensions from individual mice per experimental group were seeded in 96-well round-bottom plates and cultured for 4 hours with Leukocyte Activation Cocktail containing premixed PMA, ionomycin and brefeldin A (0.4 μL per 0.2 mL per well; BD Biosciences). After restimulation, cells were stained with fixable viability dye (Thermo Fisher) and surface-stained with fluoro-chrome-conjugated antibodies. Cells were then fixed and permeabilized using the Foxp3 Fix-Perm buffer set (eBioscience, Thermo Fisher) and stained with antibodies against IFNγ, TNFα, and Foxp3. Data were acquired on a BD LSRFortessa and analyzed using BD FACSDiva software.

NanoString gene-expression profiling.—Tumor suspensions were enriched for CD8$^+$ T cells using mouse CD8$^+$ TIL microbeads (Miltenyi Biotec) on the autoMACS Pro system (Miltenyi Biotec). RNA was extracted from 10^4 enriched CD8$^+$ TILs (equivalent to 100 ng RNA) using the RNeasy Mini Kit (Qiagen) and quantified using the NanoDrop (Thermo Fisher). Up to 100 ng of purified RNA was resuspended in 5 μL RNAse-free water and hybridized (16 hours at 65° C) with the NanoString mouse Pan-Cancer Immune Profiling panel codeset (750 endogenous genes and 20 housekeeping genes) and a custom panel-plus codeset (30 endogenous genes including PVRIG and DNAM-1). Following a fully automated processing of the hybridized probe-transcript complexes on the nCounter Prep Station (NanoString Technologies), immobilized barcodes representing all 800 targets were scanned by the nCounter Digital Analyzer (NanoString Technologies). Data were

normalized using the geNorm algorithm and groups were compared using the advanced analysis module (version 2.0.115) of nSolver 4.0 Analysis Software (NanoString Technologies).

Results

Mouse PVRIG is inducible upon activation of CD8$^+$ T cells

In the physiologic setting, human *Pvrig* is detectable in circulating NK, NKT, γδ, CD8$^+$, and to a lesser extent in CD4$^+$ T cells (10). When we examined the steady-state expression profile in mouse cells by quantitative PCR, *Pvrig* transcripts were abundant in NK and NKT cells, barely detectable in CD4$^+$ and CD8$^+$ T cells, and absent in B cells (Fig. 1A). When activated *in vitro*, mouse CD8$^+$ T cells upregulated *Pvrig* expression, although at a much slower rate compared with a related checkpoint, *Tigit* (Fig. 1B). Next, we confirmed that recombinant mouse PVRIG (mPVRIG) could bind to mouse PVRL2 (mPVRL2) protein by SPR and ELISA performed in several assay orientations (Supplementary Fig. S1A–S1D). We also observed an interaction between mPVRIG and mouse PVR (mPVR), although the affinity of mPVRIG for mPVR was 10-fold lower than the interaction between mPVRIG and mPVRL2 (Supplementary Fig. S1E). To determine whether mPVR or mPVRL2 is the dominant ligand for mPVRIG, we then tested the binding of a recombinant protein (comprised of the extracellular domain of mPVRIG fused to the Fc portion of immunoglobulin (PVRIG Fc) to B16F10 cells, which endogenously express mPVR and mPVRL2 (20). The dose-dependent binding of PVRIG Fc to B16F10 cells was inhibited by 100% following mPVRL2 siRNA knockdown but was reduced by only 33% following mPVR knockdown (Supplementary Fig. S1F–S1G), suggesting that a weak interaction occurs between mPVRIG and mPVR. Taken together, these results demonstrate that in mice, PVRL2 is the primary ligand for PVRIG.

PVRIG-deficient T cells become effectors more rapidly *in vitro*

To delineate the role of PVRIG in immune responses, we generated PVRIG-deficient mice (PVRIG$^{-/-}$; Supplementary Fig. S2). PVRIG$^{-/-}$ mice were born at the expected Mendelian ratios, displayed no overt phenotype up to 10 months of age, and at 8 weeks of age had similar leukocyte cellularity (peripheral and lymphoid tissue) when compared with wild-type mice (Supplementary Fig. S3A–S3I). Using anti-PVRIG, we found that NK cells and *in vitro*-activated wild-type CD8$^+$ T cells express PVRIG, whereas activated CD4$^+$ T cells do not. No expression of PVRIG was detected on PVRIG$^{-/-}$ cells (Fig. 1C). To examine the role of PVRIG in regulating mouse T-cell responses, we examined the proliferation of wild-type and PVRIG$^{-/-}$ T cells in two assay systems. Wild-type or PVRIG$^{-/-}$ splenocytes were activated with immobilized anti-CD3 in the presence of soluble PVRL2-Fc or control Fc protein. Soluble PVRL2-Fc significantly inhibited wild-type but not PVRIG$^{-/-}$ T-cell proliferation (Fig. 1D), corroborating an inhibitory function for mPVRIG. To evaluate the role of mPVRIG in antigen-specific CD8$^+$ T-cell responses, PVRIG$^{-/-}$ mice were bred to pmel-1 TCR transgenic mice, which express a transgenic TCR specific for gp100$_{25–33}$ (21). Pmel-1 PVRIG$^{-/-}$ Pmel-1 CD8$^+$ T-cell function was assessed following peptide stimulation and subsequent coculture with B16-F10/mhgp100 cells that constitutively express PVRL2. CD8$^+$ T cells from Pmel-1 TCR-PVRIG$^{-/-}$ mice showed enhanced degranulation and

production of effector cytokines (IFNγ and TNFα) compared with wild-type Pmel-1 $CD8^+$ T cells (Fig. 1E). Collectively, our *in vitro* analyses suggested that murine PVRIG is an inhibitory T-cell receptor that suppresses antigen-specific activity of $CD8^+$ T cells in a PVRL2-dependent manner.

PVRIG$^{-/-}$ mice mount stronger antigen-specific T effector responses against LmOva

T-cell progression is thought to be dependent on antigenic signal strength, resulting in the generation of effector T cells and eventual seeding of the memory pool (22). To investigate whether PVRIG deficiency had an impact on T-cell progression, we analyzed $CD8^+$ T-cell responses to infection with ovalbumin-expressing double-attenuated *L. monocytogenes* (LmOva; Fig. 2A). We found that relative to wild-type mice, PVRIG$^{-/-}$ mice exhibited significantly higher IFNγ-producing and IFNγ/TNFα coproducing Ova-specific $CD8^+$ T effector-cell responses on day 7 following primary immunization (Fig. 2B and C). Memory $CD8^+$ T-cell development appeared to be unaffected in PVRIG$^{-/-}$ mice relative to wild-type mice, as evidenced by comparable antigen-elicited cytokine production by both splenic (Supplementary Fig. S4A) and marrow-resident (Supplementary Fig. S4B) memory $CD8^+$ T cells in response to a secondary immunization with LmOva 2 months after the initial immunization. SIINFEKL-tetramer$^+$ $CD8^+$ T-cell frequencies were comparable between LmOva-immunized wild-type and PVRIG$^{-/-}$ mice, suggesting antigen priming was not responsible for the PVRIG-deficient phenotype (Supplementary Fig. S4C).

Tumor growth inhibition in PVRIG$^{-/-}$ mice driven by effector $CD8^+$ T cells

We next studied the effects of PVRIG deficiency on tumor growth in the immunogenic MC38 syngeneic model. PVRIG$^{-/-}$ mice displayed significantly reduced tumor growth compared with wild-type mice ($P < 0.05$; Fig. 3A and B). The tumor growth in PVRIG$^{-/-}$ mice appeared to be slower beginning day 20 after implantation. By day 24, volumes were significantly different compared with wild-type tumors. In pilot studies performed with the weakly immunogenic B16F10 melanoma model, we observed similar tumor growth inhibition in PVRIG-deficient mice ($P < 0.05$; Supplementary Fig. S5). We next analyzed MC38 tumor, spleen, draining and nondraining lymph nodes for cytokine production in response to stimulation with p15E peptide or PMA plus ionomycin. The endogenous retroviral envelope protein p15E, first characterized on B16 melanoma, is also expressed by MC38 cells (23). The optimal *in vitro* stimulation dose for p15E peptide was titrated in pilot experiments with B16F10 tumors. $CD8^+$ T cells from tumors but not from spleen, draining, or nondraining lymph nodes produced cytokines (IFNγ and TNFα) in response to p15E peptide stimulation (Fig. 3C and D). We observed a significant accumulation of IFNγ$^+$ p15E-specific $CD8^+$ effectors in PVRIG$^{-/-}$ tumors as compared with wild-type tumors (Fig. 3C and D; $P = 0.012$). With PMA and ionomycin stimulation, cytokine production by $CD8^+$ T cells from PVRIG$^{-/-}$ tumors as well as spleens was elevated compared with wild-type tissues (Fig. 3E and F; $P = 0.003$ and $P = 0.06$, respectively). The role of PVRIG-deficient effector $CD8^+$ T cells in antitumor immunity was corroborated by data showing that depletion of $CD8^+$ T cells resulted in accelerated tumor growth in both PVRIG$^{-/-}$ and wild-type mice (Supplementary Fig. S6).

PVRIG$^{-/-}$ CD8^{+} TILs have an inflammatory, cytotoxic signature

To characterize the molecular basis of PVRIG$^{-/-}$ TIL activation relative to wild-type TILs, we performed NanoString-based transcriptomic analysis of enriched tumor-infiltrating CD8^{+} T cells from day 18 MC38 tumors. For our analyses, 30 additional gene targets, including DNAM-1 and PVRIG, were added to the 770-gene nCounter mouse pan-cancer immune profiling panel (NanoStringTechnologies). Using a cutoff of an adjusted *P* value or false discovery rate (FDR) < 0.5, 145 of 780 endogenous targets were found to be significantly upregulated or downregulated in PVRIG$^{-/-}$ CD8^{+} TILs relative to wild-type TILs on day 18 (Fig. 4A). Of these 145 genes, 89 were upregulated and 56 were downregulated in PVRIG$^{-/-}$ CD8^{+} TILs (Fig. 4A; Supplementary File S1). In the settings of viral infection, inhibitory receptors induced upon T-cell activation are transiently upregulated on effector T cells but are rapidly downregulated following viral clearance (24). In the MC38 tumor model, we found that CD8^{+} T cells infiltrating PVRIG$^{-/-}$ tumors highly expressed several inhibitory receptors, including TIGIT, Tim-3 (*Havcr2*), PD-1 (*Pdcdl*), and LAG-3 (*Lag3*), compared with wild-type CD8^{+} T cells (Fig. 4A; Supplementary File S1). Genes with cytotoxic or cytolytic functions such as granzyme A, granzyme B, and perforin were upregulated in PVRIG$^{-/-}$ CD8^{+} TILs compared with wild-type CD8^{+} TILs (Fig. 4A; Supplementary File S1). Gene set analyses revealed significant upregulation of genes belonging to the CD28 costimulation family (Fig. 4B) as well as the interleukin signaling pathways (Fig. 4C) in PVRIG$^{-/-}$ CD8^{+} TILs compared with wild-type CD8^{+} TILs. A panel of select genes encoding inflammatory cytokines, transcription factors, activating and inhibitory receptors (IFNγ, granzymes A and B, perforin, TIGIT, PD-1, CTLA-4, Tim-3, and DNAM-1) was also validated by TaqMan qRT-PCR (Supplementary Fig. S7). PVRIG$^{-/-}$ CD8^{+} TILs did not appear to upregulate DNAM-1 (CD 226) transcripts (Supplementary Fig. S7). PVRIG$^{-/-}$ CD8^{+} TILs, thus, have a cytotoxic gene-rich transcriptional signature, endowing them with their observed tumoricidal capability. The cytotoxic gene expression was also associated with upregulated activation-induced inhibitory receptors (Fig. 4D), suggesting that the PVRIG$^{-/-}$ phenotype may be more responsive to checkpoint inhibitor combination therapy.

PD-L1 blockade inhibits established MC38 tumors in PVRIG$^{-/-}$ mice

On day 18 after implantation, MC38 tumors in PVRIG$^{-/-}$ mice were infiltrated by TNFα-producing myeloid (CD11b^{+}) cells that were significantly elevated compared with wild-type tumors (Supplementary Fig. S8; $P = 0.02$). Relative to splenic myeloid cells that expressed PVR but no PVRL2 (Supplementary Fig. S9A), 46% (PVRIG$^{-/-}$) and 48% (wild-type) of tumor-infiltrating myeloid cells coexpressed PVRL2 and PVR, whereas the corresponding percentages in tumor cells were 10% and 21%, respectively (Supplementary Fig. S9B and S9C). Subsequently, in a pilot study performed on day 25 MC38 tumors, we analyzed PD-L1 expression by flow cytometry and found a significant increase in PD-L1 geometric mean fluorescence on PVRIG$^{-/-}$ relative to wild-type myeloid cells (Fig. 5A). This suggested PD-L1 was upregulated on PVRIG$^{-/-}$ tumor-associated myeloid cells in response to the copious IFNγ produced within the TME by the PVRIG$^{-/-}$ CD8 effectors (Fig. 3C and D) and mirrors the adaptive resistance mechanism of immune escape in clinical tumors (25). Therefore, we hypothesized that PD-L1 blockade timed to coincide roughly with its expected surface upregulation on myeloid cells in the TME on day 25 would yield an optimal combination regimen in PVRIG$^{-/-}$ mice. Anti-PD-L1 or rat IgG2b isotype was

administered to both wild-type and PVRIG$^{-/-}$ mice bearing established MC38 tumors on day 25. PD-L1 blockade, begun on day 25, was effective only in PVRIG-deficient mice ($P < 0.0001$, compared with wild-type; Fig. 5B). Wild-type mice did not respond to anti-PD-L1 treatment and succumbed to tumor-related morbidity by day 34, whereas 63% of PVRIG$^{-/-}$ mice were alive on day 38 (Fig. 5C). Isotype-treated wild-type mice did not survive beyond day 31, whereas 40% of the isotype-treated PVRIG$^{-/-}$ animals persisted until day 38 (Fig. 5C).

PD-L1 blockade synergizes with PVRIG deletion in reducing tumor growth

The concomitant upregulation of PD-1 on CD8^{+} TIL along with PD-L1 on myeloid cells in PVRIG-deficient tumors prompted us to investigate whether treatment with a PD-1 pathway blocker (anti-PD-L1) could confer additional tumor growth inhibition in PVRIG$^{-/-}$ mice. Dose and treatment schedule for PD-L1 blockade was optimized before experiments were performed, as we observed that a regimen of four 200 μg doses (3 days apart) initiated on day 8 after tumor implantation was curative in the MC38 model. Thus, an optimized regimen of anti-PD-L1 (4 doses of 100 μg, 3 days apart) was administered beginning day 14, which reduced tumor growth in PVRIG$^{-/-}$ mice compared with anti-PD-L1-treated wild-type mice ($P = 0.052$; Fig. 6A and B). Isotype-treated PVRIG$^{-/-}$ mice had significantly smaller tumors compared with isotype-treated wild-type mice on day 27 ($P < 0.05$; Fig. 6A and B). To assess the functional effects of PD-L1 blockade on the TME in the context of PVRIG deletion, we analyzed tumors from isotype/anti-PD-L1-treated wild-type and PVRIG$^{-/-}$ mice on day 18, when groups had received 2 doses of isotype/anti-PD-L1. Both in the presence and absence of PD-L1 blockade, tumors from PVRIG$^{-/-}$ animals had greater infiltration of immune cells in general (Fig. 6C) and CD8^{+} T cells in particular (Fig. 6D). Intratumoral NK cells were comparable between wild-type and PVRIG$^{-/-}$ mice, regardless of anti-PD-L1 treatment (Fig. 6E). Cytokine-producing CD8^{+} T cells were also elevated in PVRIG$^{-/-}$ tumors compared with wild-type tumors, significantly more so in the absence of PD-L1 blockade (Fig. 6F and G). The enhanced immune function in PVRIG-null tumors, particularly following PD-L1 blockade, was mirrored in PVRIG-null tumor-draining lymph nodes that had increased IFNγ^{+}/TNFα^{+} effector CD8^{+} T cells relative to wild-type controls (Fig. 6H). Taken together, these data demonstrate that PVRIG ablation combined with PD-L1 blockade amplifies antitumor immunity resulting in reduced tumor growth.

Anti-mPVRIG treatment reduces tumor growth in combination with anti-PD-L1

After demonstrating reduced tumor growth in PVRIG$^{-/-}$ mice, we next examined whether therapeutic treatment with an anti-PVRIG blocking Ab, alone or in combination with anti-PD-L1, could result in a similar effect on tumor growth. To this end, we generated high-affinity (0.33–0.39 nmol/L) anti-mPVRIG and confirmed its specificity (Supplementary Fig. S10A–S10C). Anti-mPVRIG disrupted the mPVRIG-mPVRL2 interaction by inhibiting the binding of mPVRIG Fc to B16-F10 cells that endogenously express PVRL2 (Supplementary Fig. S10D) and the binding of mPVRL2 Fc to mPVRIG-transfected HEK293 cells (Supplementary Fig. S10E). Next, we tested the *in vivo* efficacy of this Ab in the BALB/c CT26 colon carcinoma model. Treatment of tumor-bearing BALB/c mice with anti-mPVRIG or anti-PD-L1 as monotherapy failed to reduce tumor growth. However, the combined regimen of anti-PVRIG and anti-PD-L1 delayed CT26 tumor growth (Fig. 6I) and

significantly increased the survival of treated mice, with 4 of 10 mice surviving past 80 days (Fig. 6J). These data demonstrate that combination of PD-1 and PVRIG inhibitors can reduce the growth of tumors that are refractory to either as monotherapy.

Discussion

Within the immunoglobulin (Ig) superfamily, encompassing more than 700 glycoprotein genes in the human genome (26), only a few function as T-cell inhibitory receptors. Using computational algorithms, we have predicted immune checkpoints based on genomic and proteomic attributes shared with known immune checkpoints, such as gene structure, protein domains, predicted cellular localization and expression patterns. One of the checkpoint candidates that emerged from our discovery process was PVRIG (27). Zhu and colleagues (10) have shown that human PVRIG (CD112R) can inhibit T-cell function through an interaction with its cognate ligand, PVRL2; these findings have, therefore, validated our *in silico* prediction tools. However, the *in vivo* role of PVRIG in immune modulation and the potential relevance of the PVRIG-PVRL2 axis as a functional checkpoint particularly in tumor-driven immune evasion have not been reported. Complementing our efforts at characterizing the PVRIG-PVRL2 pathway in the human TME (27), this study addresses the role of murine PVRIG in the contexts of activation-induced coinhibition, $CD8^+$ effector differentiation during acute bacterial infection, and, lastly, syngeneic tumor models.

PVRIG is a member of the nectin and nectin-like family, placing it among several known immunoregulatory receptors in the family. Of these receptors, DNAM, TIGIT, and CD96 are most closely related to PVRIG as they share the same ligands, PVR and PVRL2 (8). Examining the interplay of the receptors within this family is crucial to understanding the relevance and mechanism of action of PVRIG. We observed that PVRIG displayed late induction of transcript and protein expression post-T-cell activation as compared with TIGIT. In addition to differences in expression, TIGIT and PVRIG bind differentially to PVR and PVRL2. TIGIT is reported to bind to PVR and weakly to PVRL2 and PVRL3 (8, 9). We were unable to detect an interaction between TIGIT and PVRL2 using ELISA or SPR, suggesting that PVR is the dominant ligand for TIGIT. At the same time, we detected a high-affinity interaction between PVRL2 and PVRIG, indicating that PVRIG is the dominant inhibitory receptor for PVRL2. *In vivo*, we did not detect PVRL2 in steady-state myeloid cells but found it to be expressed mainly by tumor-infiltrating myeloid cells and by a smaller subpopulation of tumor cells. Although past studies have demonstrated that ectopic PVRL2/PVR expression on tumors induces DNAM-1-mediated cytotoxicity (28) and PVRL2 gene expression is elevated in methylcholanthrene-induced tumors from PVR-deficient mice (29), surface PVRL2 expression in the TME from preclinical models has not been reported. An immunosuppressive role has been shown for PVR-expressing host myeloid cells, distinct from PVR^+ tumor cells (30). The precise immunologic role of intratumoral $PVRL2^+$ myeloid cells, a subset of the PVR^+ myeloid population, remains to be characterized, particularly in regard to whether the dominant PVRL2-PVRIG signaling pathway could be supplanted by the low-affinity PVR-PVRIG interaction. Thus, the functional role of PVRIG within this family is through a high-affinity interaction with PVRL2, high expression on effector $CD8^+$ T cells, and a delayed induction profile compared with TIGIT. These data further suggest that on lymphocytes that coexpress both receptors,

TIGIT and PVRIG are parallel rather than overlapping signaling nodes in this axis and that blocking both could promote tumor-infiltrating T-cell activation.

The inducible expression of PVRIG on murine $CD8^+$ T cells as compared with TIGIT, along with its distinct kinetics and sustained late expression, mirrors its expression pattern in humans and suggests a nonredundant and conserved role for PVRIG in regulating T-cell responses. The latter was evident in $PVRIG^{-/-}$ mice generating more $CD8^+$ T effector cells when acutely infected with attenuated ovalbumin-expressing *Listeria monocytogenes*. When the effector populations entered the contraction phase, post-reinfection memory T-cell responses were comparable between $PVRIG^{-/-}$ and wild-type mice. IL12 signaling via its cognate receptor on $CD8^+$ T cells skews their differentiation toward activated effector cells and negatively regulates the generation of $CD8^+$ memory precursors (31, 32). The $PVRIG^{-/-}$ $CD8^+$ TIL transcriptome revealed upregulation of the IL12 receptor (IL12rb2; Supplementary File S1), suggesting the PVRIG-null phenotype is more responsive to inflammatory cues emanating from bacterial infection or from within the TME.

Using PVRIG-deficient mice and antagonistic anti-PVRIG antibodies, we demonstrate a role of PVRIG in regulating antitumor T-cell responses. In mice, as in humans, PVRIG expression was observed in steady-state NK and NKT cells and induced upon activation in *ex vivo* $CD8^+$ T lymphocytes as well as tumor-infiltrating $CD8^+$ T lymphocytes. Subsequently, immune T-cell checkpoint activity of mouse PVRIG was demonstrated by increased proliferation and effector function of T cells derived from $PVRIG^{-/-}$ mice compared with wild-type mice. Moreover, reduced tumor growth was evident in $PVRIG^{-/-}$ mice and was attributable largely to tumor-infiltrating effector $CD8^+$ responses. Tumor growth inhibition observed in $PVRIG^{-/-}$ mice was further enhanced when an anti-PD-L1 was administered. Immune monitoring analysis in anti-PD-L1-treated $PVRIG^{-/-}$ mice showed increased $CD8^+$ T-cell responses, with the greatest increase detected in the draining lymph node at day 18 after treatment. We further demonstrate that an antagonistic Ab to PVRIG reduced tumor growth when combined with anti-PD-L1, showing the effects of blocking PVRIG in a therapeutic setting. These data provide *in vivo* proof of concept using preclinical tumor models that targeting PVRIG in combination with an additional checkpoint such as PD-1 is a potential therapy for the treatment of cancers.

In summary, our study provides several insights into PVRIG biology by characterizing the expression of this PVRIG-PVRL2 axis in preclinical models, demonstrating a role for PVRIG in regulating the tumor-infiltrating $CD8^+$ T-cell cytotoxicity and showing that PVRIG antagonism in combination with PD-L1 blockade leads to a synergistic reduction in tumor growth.

Supplementary Material

Refer to Web version on PubMed Central for supplementary material.

Acknowledgments

Our research was supported by grants from Compugen Ltd. (Israel), the Bloomberg-Kimmel Institute for Cancer Immunotherapy, and the NIH (Cancer Center Support Grant P30 CA006973).

References

1. Hanahan D, Weinberg RA. Hallmarks of cancer: the next generation. Cell 2011;144:646–74. [PubMed: 21376230]
2. Beatty GL, Gladney WL. Immune escape mechanisms as a guide for cancer immunotherapy. Clin Cancer Res 2015;21:687–92. [PubMed: 25501578]
3. Pennock GK, Chow LQM. The evolving role of immune checkpoint inhibitors in cancer treatment. Oncologist 2015;20:812–22. [PubMed: 26069281]
4. Hodi FS, O'Day SJ, McDermott DF, Weber RW, Sosman JA, Haanen JB, et al. Improved survival with ipilimumab in patients with metastatic melanoma. N Engl J Med 2010;363:711–23. [PubMed: 20525992]
5. Brahmer JR, Tykodi SS, Chow LQ, Hwu WJ, Topalian SL, Hwu P, et al. Safety and activity of anti-PD-L1 antibody in patients with advanced cancer. N Engl J Med 2012;366:2455–65. [PubMed: 22658128]
6. Topalian SL, Hodi FS, Brahmer JR, Gettinger SN, Smith DC, McDermott DF, et al. Safety, activity, and immune correlates of anti-PD-1 antibody in cancer. N Engl J Med 2012;366:2443–54. [PubMed: 22658127]
7. Jenkins RW, Barbie DA, Flaherty KT. Mechanisms of resistance to immune checkpoint inhibitors. Br J Cancer 2018;118:9. [PubMed: 29319049]
8. Chan CJ, Andrews DM, Smyth MJ. Receptors that interact with nectin and nectin-like proteins in the immunosurveillance and immunotherapy of cancer. Curr Opin Immunol 2012;24:246–51. [PubMed: 22285893]
9. Martinet L, Smyth MJ. Balancing natural killer cell activation through paired receptors. Nat Rev Immunol 2015;15:243–54. [PubMed: 25743219]
10. Zhu Y, Paniccia A, Schulick AC, Chen W, Koenig MR, Byers JT, et al. Identification of CD112R as a novel checkpoint for human T cells. J Exp Med 2016;213:167–76. [PubMed: 26755705]
11. Bottino C, Castriconi R, Pende D, Rivera P, Nanni M, Carnemolla B, et al. Identification of PVR (CD155) and Nectin-2 (CD112) as cell surface ligands for the human DNAM-1 (CD226) activating molecule. J Exp Med 2003;198:557–67. [PubMed: 12913096]
12. Yu X, Harden K, Gonzalez LC, Francesco M, Chiang E, Irving B, et al. The surface protein TIGIT suppresses T cell activation by promoting the generation of mature immunoregulatory dendritic cells. Nat Immunol 2009;10:48–57. [PubMed: 19011627]
13. Stanietsky N, Sim ic H, Arapovic J, Toporik A, Levy O, Novik A, et al. The interaction of TIGIT with PVR and PVRL2 inhibits human NK cell cytotoxicity. Proc Natl Acad Sci USA 2009;106:17858–63. [PubMed: 19815499]
14. Johnston RJ, Comps-Agrar L, Hackney J, Yu X, Huseni M, Yang Y, et al. The immunoreceptor TIGIT regulates antitumor and antiviral CD8(+) T cell effector function. Cancer Cell 2014;26:923–37. [PubMed: 25465800]
15. Zhang B, Zhao W, Li H, Chen Y, Tian H, Li L, et al. Immunoreceptor TIGIT inhibits the cytotoxicity of human cytokine-induced killer cells by interacting with CD155. Cancer Immunol Immunother 2016;65:305–14. [PubMed: 26842126]
16. Xu F, Sunderland A, Zhou Y, Schulick RD, Edil BH, Zhu Y. Blockade of CD112R and TIGIT signaling sensitizes human natural killer cell functions. Cancer Immunol Immunother 2017;66:1367–75. [PubMed: 28623459]
17. Chan CJ, Martinet L, Gilfillan S, Souza-Fonseca-Guimaraes F, Chow MT, Town L, et al. The receptors CD96 and CD226 oppose each other in the regulation of natural killer cell functions. Nat Immunol 2014;15:431–8. [PubMed: 24658051]
18. Fuchs A, Cella M, Giurisato E, Shaw AS, Colonna M. Cutting edge: CD96 (tactile) promotes NK cell-target cell adhesion by interacting with the poliovirus receptor (CD155). J Immunol 2004;172:3994–8. [PubMed: 15034010]
19. Altman JD, Davis MM. MHC-Peptide Tetramers to Visualize Antigen-Specific T Cells. Curr Protoc Immunol 2016;115:17.3.1–.3.44. [PubMed: 27801510]

20. Kurtulus S, Sakuishi K, Ngiow SF, Joller N, Tan DJ, Teng MW, et al. TIGIT predominantly regulates the immune response via regulatory T cells. J Clin Invest 2015;125:4053–62. [PubMed: 26413872]
21. Overwijk WW, Tsung A, Irvine KR, Parkhurst MR, Goletz TJ, Tsung K, et al. gp100/pmel 17 is a murine tumor rejection antigen: induction of "self"-reactive, tumoricidal T cells using high-affinity, altered peptide ligand. J Exp Med 1998;188:277–86. [PubMed: 9670040]
22. Lanzavecchia A, Sallusto F. Progressive differentiation and selection of the fittest in the immune response. Nat Rev Immunol 2002;2:982. [PubMed: 12461571]
23. Zeh HJ, Perry-Lalley D, Dudley ME, Rosenberg SA, Yang JC. High Avidity CTLs for two self-antigens demonstrate superior in vitro and in vivo antitumor efficacy. J Immunol 1999;162:989. [PubMed: 9916724]
24. Wherry EJ, Ha SJ, Kaech SM, Haining WN, Sarkar S, Kalia V, et al. Molecular signature of CD8+ T cell exhaustion during chronic viral infection. Immunity 2007;27:670–84. [PubMed: 17950003]
25. Taube JM, Anders RA, Young GD, Xu H, Sharma R, McMiller TL, et al. Colocalization of inflammatory response with B7-h1 expression in human melanocytic lesions supports an adaptive resistance mechanism of immune escape. Sci Transl Med 2012;4:127ra37.
26. International Human Genome Sequencing Consortium. Initial sequencing and analysis of the human genome. Nature 2001;409:860–921. [PubMed: 11237011]
27. Whelan S, Ophir E, Kotturi MF, Levy O, Ganguly S, Leung L, et al. PVRIG and PVRL2 are induced in cancer and inhibit CD8+ T cell function. Cancer Immunol Res 2019;7:257–68. [PubMed: 30659054]
28. Tahara-Hanaoka S, Shibuya K, Kai H, Miyamoto A, Morikawa Y, Ohkochi N, et al. Tumor rejection by the poliovirus receptor family ligands of the DNAM-1 (C D 226) receptor. Blood 2006;107:1491–6. [PubMed: 16249389]
29. Nagumo Y, Iguchi-Manaka A, Yamashita-Kanemaru Y, Abe F, Bernhardt G, Shibuya A, et al. Increased CD112 expression in methylcholanthrene-induced tumors in CD155-deficient mice. PLoS ONE 2014;9:e112415. [PubMed: 25384044]
30. Li XY, Das I, Lepletier A, Addala V, Bald T, Stannard K, et al. CD155 loss enhances tumor suppression via combined host and tumor-intrinsic mechanisms. J Clin Invest 2018;128:2613–25. [PubMed: 29757192]
31. Pearce EL, Shen H. Generation of CD8 T cell memory is regulated by IL-12. J Immunol 2007;179:2074–81. [PubMed: 17675465]
32. Gourley TS, Wherry EJ, Masopust D, Ahmed R. Generation and maintenance of immunological memory. Sem Immunol 2004;16:323–33.

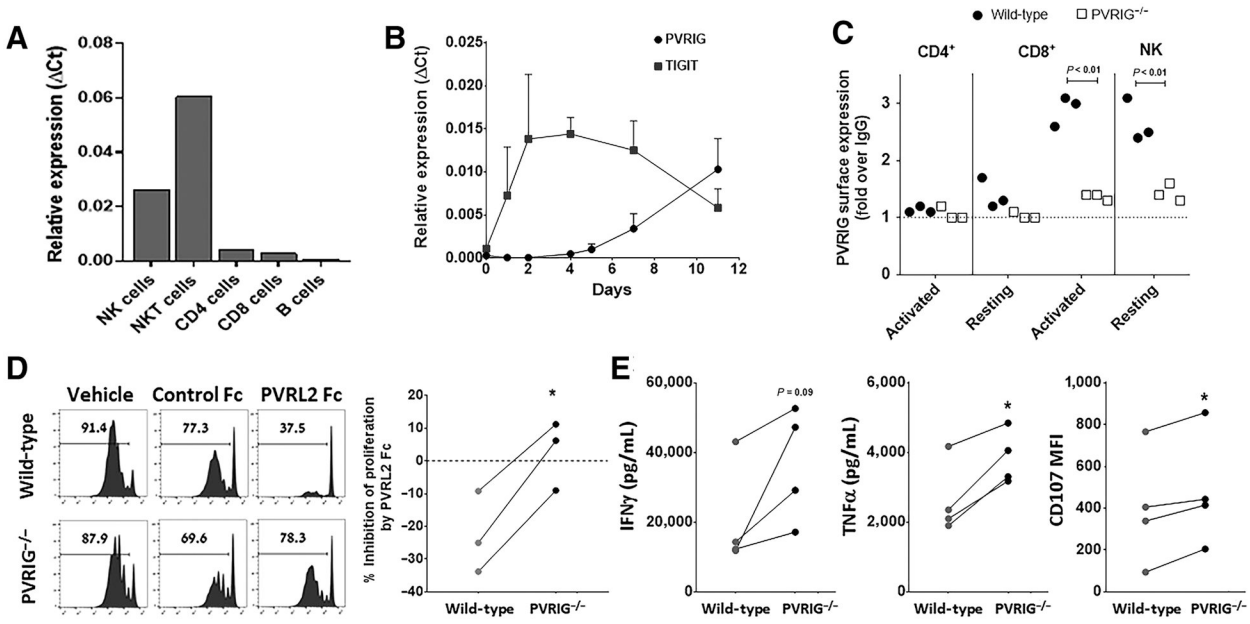

Figure 1.

PVRIG-deficient mice have increased T-cell function. **A**, RNA expression of PVRIG was assessed by qRT-PCR from purified mouse immune-cell subsets. Relative expression of the housekeeping gene, RPL18, was determined by the ΔCT method. One of two experiments performed is represented here. **B**, Pmel-1 $CD8^+$ TCR transgenic T cells were activated with gp100 (25–33) peptide. PVRIG and TIGIT RNA transcripts were analyzed by qRT-PCR at the indicated time points. The graph shows mean ± SEM of results from five different experiments. **C**, Spleens were harvested from $PVRIG^{-/-}$ and wild-type littermates and analyzed by FACS for expression of PVRIG on $CD8^+$ T and NK cells *ex vivo* ("resting" cells). In addition, $CD3^+$ splenic T cells were activated for 11 days with anti-CD3/anti-CD28 beads. Following the activation, PVRIG expression on $CD4^+$ and $CD8^+$ T cells ("activated" cells) was analyzed by flow cytometry. Cells were gated based on viability-dye exclusion followed by gating on $CD3^-/CD49b^+$, $CD3^+/CD4^+$, and $CD3^+/CD8^+$ for acquisition of NK, $CD4^+$ T, and $CD8^+$ T cells. Each dot represents cells derived from an individual mouse. **D**, Wild-type and $PVRIG^{-/-}$ splenocytes were labeled with Cell Proliferation Dye eFluor450 and cultured in the presence of control Fc (mouse IgG2a) or with mouse PVRL2-Fc. After 4 days of culture, cell division was analyzed by flow cytometry. Representative FACS plots from one experiment (left) and the summary of percentage inhibition by PVRL2 Fc (% inhibition of proliferation control Fc - PVRIG Fc) from three independent experiments (right) are presented. *, $P < 0.05$, paired Student *t* test for the change in proliferation in the presence of PVRL2-Fc relative to proliferation in the presence of protein control in wild-type versus $PVRIG^{-/-}$ T cells. E, Pmel-1 $CD8^+$ T cells derived from Pmel-1 $PVRIG^{-/-}$ or Pmel-1 wild-type mice were activated for 11 days with their cognate peptide and IL2. Activated Pmel-1 $CD8^+$ T cells were then cocultured with B16-Db/gp100 cells for 18 hours and evaluated for CD107 expression and for cytokine production. Four independent experiments are presented as indicated by each paired dot. *, $P < 0.05$, Student *t* test comparing $PVRIG^{-/-}$ versus wild-type.

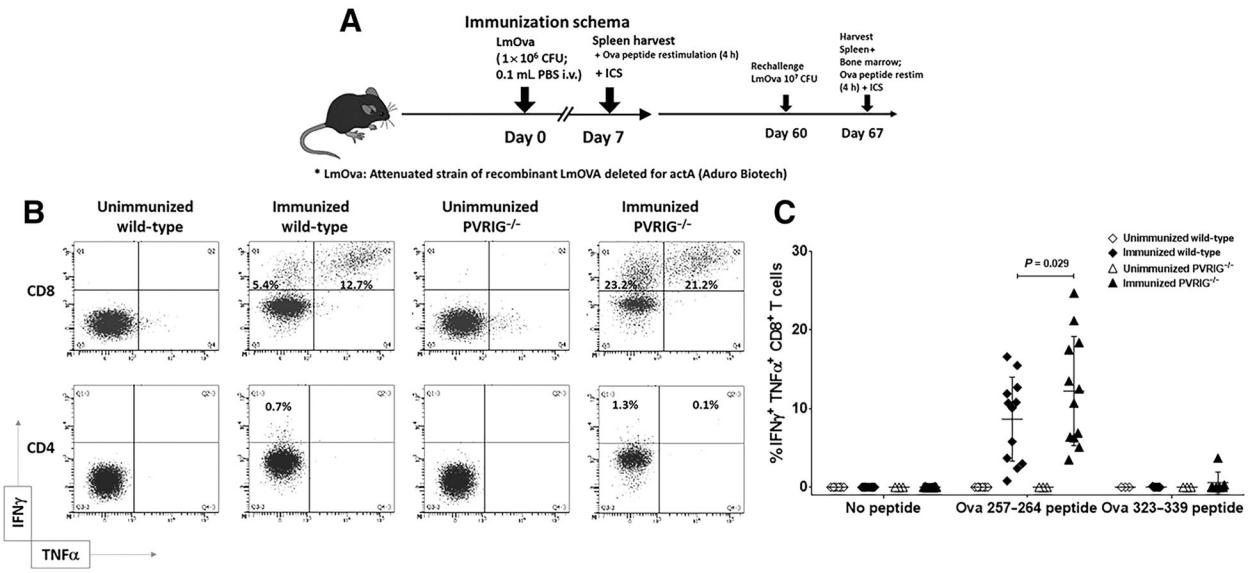

Figure 2.

PVRIG$^{-/-}$ mice display increased antigen-specific effector responses following acute *Listeria* infection. **A**, Wild-type and PVRIG$^{-/-}$ mice were immunized with attenuated Ovalbumin-expressing *Listeria monocytogenes* (LmOVA; 10^6 CFU i.v.). On day 7 After immunization, spleens were harvested, and cells were cultured with $OVA_{257–264}$ or $OVA_{323–339}$ peptide (100 ng/mL) in the presence of brefeldin A for 4 hours. Cells were then stained for surface markers and in tracellular IFNγ and TNFα. **B**, Representative dot plots of gated CD8$^+$ (top) and CD4$^+$ (bottom) T cells from unimmunized/immunized wild-type and PVRIG$^{-/-}$ mice are shown. Numbers in dot plots indicate the percentages of CD8$^+$ and CD4$^+$ T cells that produce IFNγ or both IFNγ and TNFα in response to $Ova_{257–264}$ or $Ova_{323–339}$ peptide, respectively. **C**, Graphical summary of proportions of splenic CD8$^+$ T cells from all four groups of mice coproducing IFNγ and TNFα following restimulation. Two independent experiments are shown here.

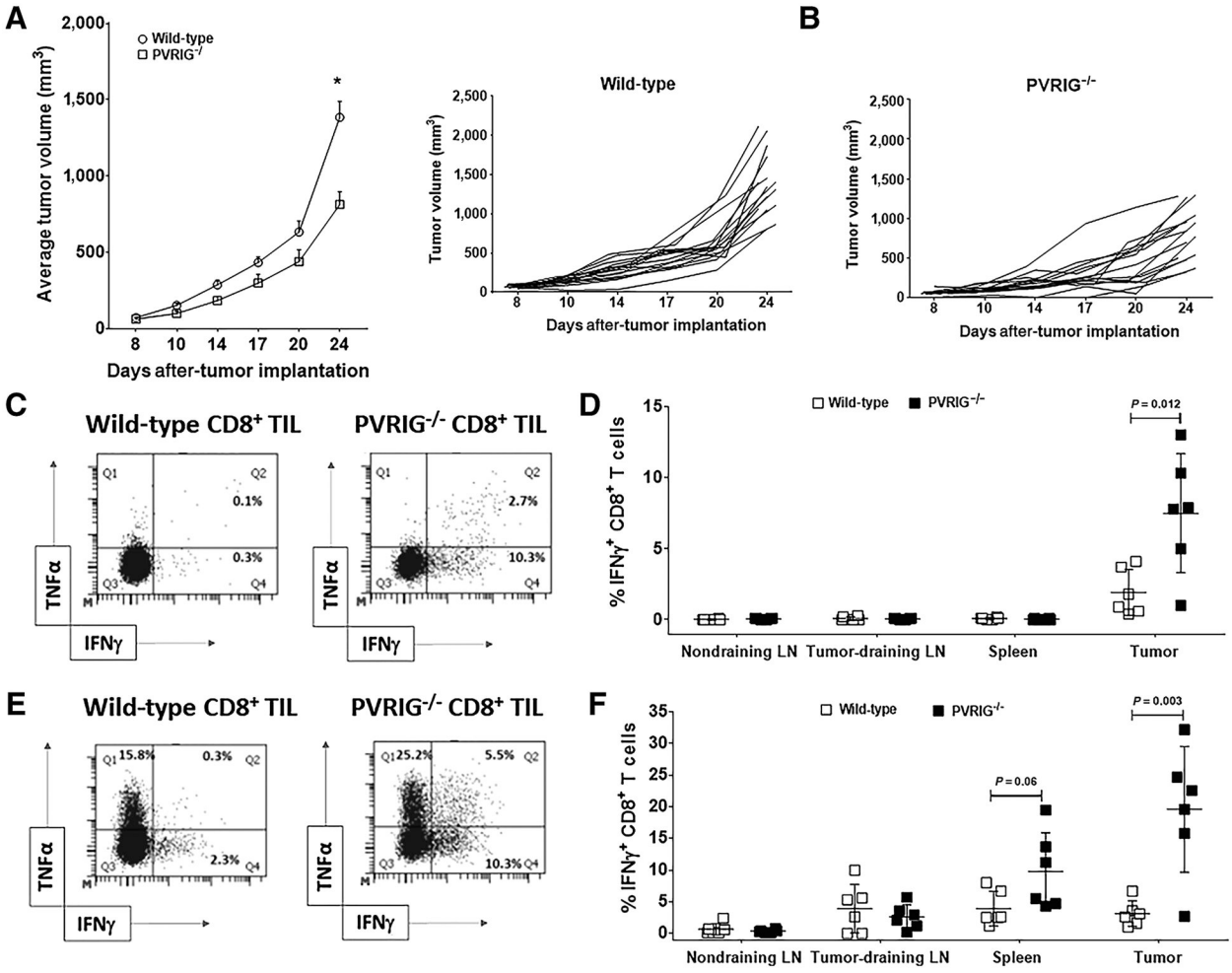

Figure 3.

PVRIG deficiency results in reduced tumor growth and increased $CD8^+$ effector T-cell functions. **A**, C57BL/6 wild-type or $PVRIG^{-/-}$ mice were subcutaneously injected with 5×10^5 MC38 cells. Tumor volumes were measured twice weekly. Two independent experiments with $n = 15$ mice per group are shown. Mean tumor volumes ± SEM are represented graphically. *, $P < 0.05$ by an unpaired Student *t* test for wild-type mice versus $PVRIG^{-/-}$ mice. **B**, Individual tumor growth curves are shown. $n = 15$ mice per group. **C**, In separate experiments, C57BL/6 wild-type or $PVRIG^{-/-}$ mice were subcutaneously implanted with 5×10^5 MC38 cells. At day 18 After implantation, mice from either cohort were sacrificed, and tumors, spleens, tumor-draining and nondraining lymph nodes were collected for *ex vivo* analyses. Dissociated tumors were enriched for $CD45^+$ cells prior to stimulation for 4 hours with either (**C–D**) p15E peptide (0.1 μg/mL) or (**E–F**) PMA and ionomycin in the presence of brefeldin A. Representative dot plots depict frequencies of $TNF\alpha^+$, $TNF\alpha^+$ $IFN\gamma^+$, and $IFN\gamma^+$ $CD8^+$ TILs from wild-type or $PVRIG^{-/-}$ mice in response to p15E peptide (**C**) or PMA and ionomycin (**E**). Corresponding graphs illustrate the percentages of $IFN\gamma^+$ $CD8^+$ TIL in wild-type and $PVRIG^{-/-}$ mice following p15E peptide (**D**) or PMA and ionomycin stimulation (**F**). Mean ± SEM is shown and *P* values from an unpaired Student *t* test are shown.

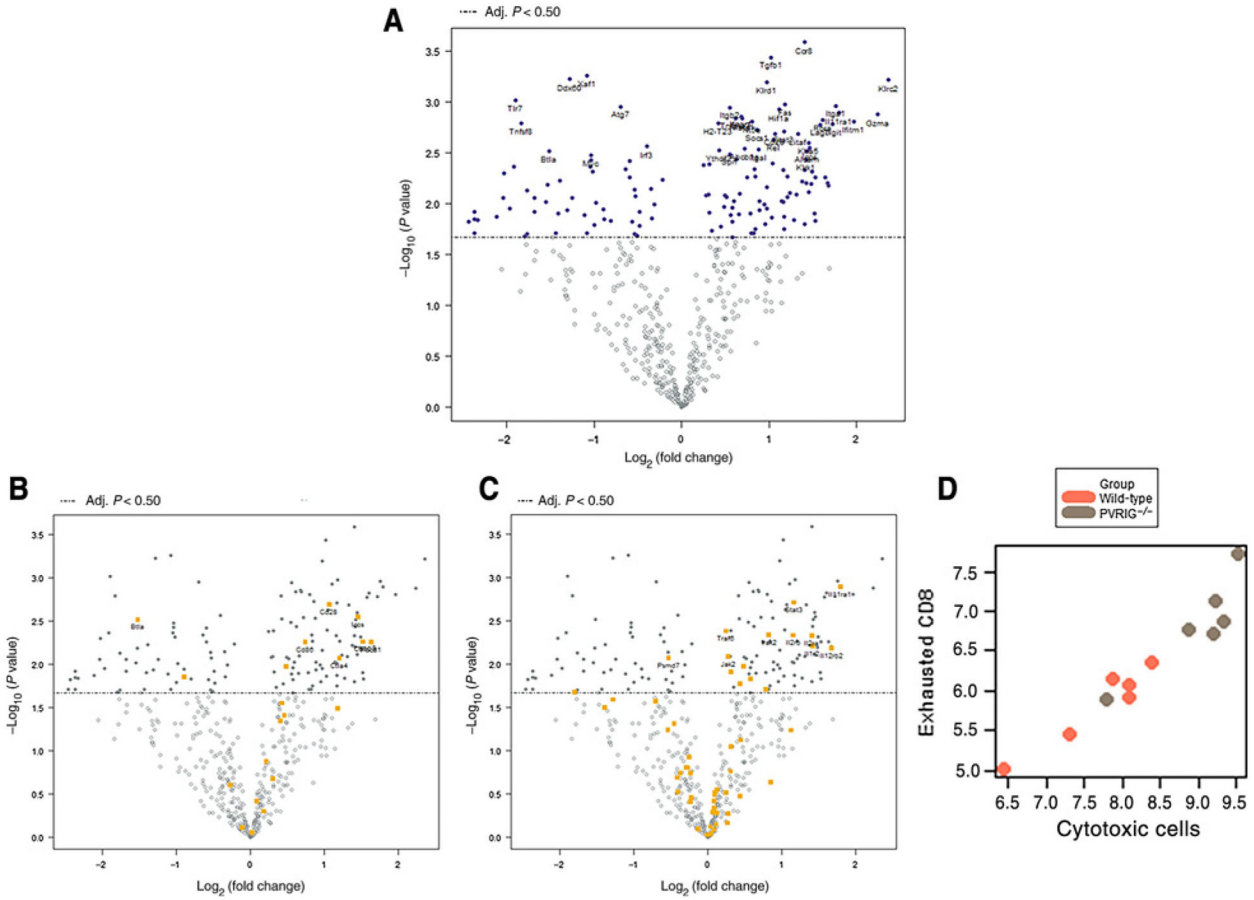

Figure 4.

PVRIG-deficient CD8$^+$ TILs have an activated effector transcriptomic profile with upregulated cytotoxic and checkpoint signatures. MC38 cells (5×10^5) were inoculated into wild-type or PVRIG$^{-/-}$ mice. On day 18, CD8$^+$ TILs were purified from tumors and RNA was extracted. CD8$^+$ TIL RNA (100 ng) was hybridized with the NanoString mouse Pan-Cancer Immune Profiling panel codeset (750 endogenous genes and 20 housekeeping genes) and a custom panel-plus codeset (30 endogenous genes including PVRIG and DNAM-1) for 16 hours, followed by automated washing and immobilization on the nCounter prep-station and subsequent scanning of aligned fluorescent barcodes on the nCounter digital scanner. Raw data were analyzed using the advanced analysis module (version 2.0.115) on nSolver 4.0 software (NanoString Technologies). **A**, Volcano plot displaying each gene's $-\log_{10}(P$ value) and $\log_2$ fold change with the selected covariate. Statistically significant genes fall at the top of the plot above the horizontal lines, and differentially expressed genes fall to either side. Horizontal line indicates an FDR threshold of 0.5. Colored genes indicate resulting P value is below the FDR threshold. The 40 most statistically significant genes are labeled in the plot. **B–C**, Volcano plots of gene set analyses displaying each gene's $-\log_{10}(P$ value) and $\log_2$ fold change for the selected covariate. Highly statistically significant genes fall at the top of the plot, and highly differentially expressed genes fall to either side. Genes with in the "Costimulation by the CD28 family" gene set (**B**) and "Signaling by Interleukins" gene set (**C**) are highlighted in orange. The horizontal line indicates an FDR threshold of 0.5. **D**,

Genes previously shown to be characteristic of cytotoxic cell populations as well as exhausted $CD8^+$ T cells have been used to measure abundance of these populations. The plot shows cytotoxic cell type measurements against exhausted $CD8^+$ T-cell abundance. Points are colored by group.

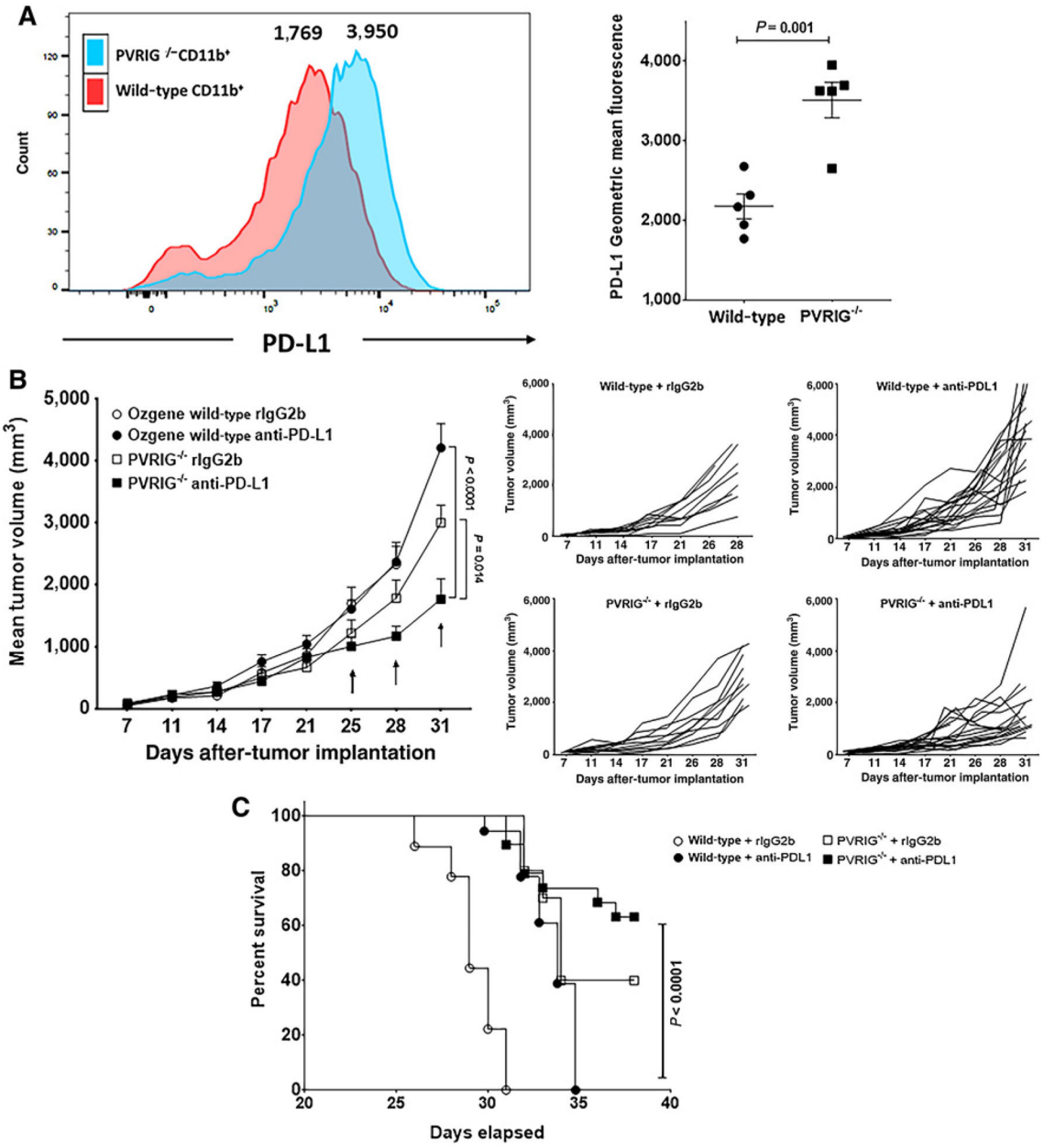

Figure 5.

PD-L1 is upregulated on tumor-infiltrating myeloid cells in PVRIG$^{-/-}$ mice. **A**, Representative overlay of PD-L1 staining on gated CD11b^{+} cells that were purified from CD45-enriched TILs on day 25 After tumor implantation. Numerical value insets indicate geometric mean fluorescence. The graph illustrates differential brightness of PD-L1 staining in PVRIG$^{-/-}$ MC38 myeloid cells relative to their wild-type counterparts. **B**, Delayed PD-L1 blockade results in inhibition of established MC38 tumors in PVRIG$^{-/-}$ mice. Wild-type and PVRIG$^{-/-}$ mice were implanted with 5×10^5 MC38 cells, and anti-PD-L1 or rat IgG2b isotype was administered every 3 days beginning day 25. Mean tumor volumes along with individual tumor growth curves for all four cohorts are shown. Arrows indicate time points of anti-PD-L1 dosing. **C**, Survival curves of MC38-bearing PVRIG$^{-/-}$ and wild-type mice

treated with anti-PD-L1 or rat IgG2b isotype beginning day 25. *P* value is from the log-rank (Mantel-Cox) test.

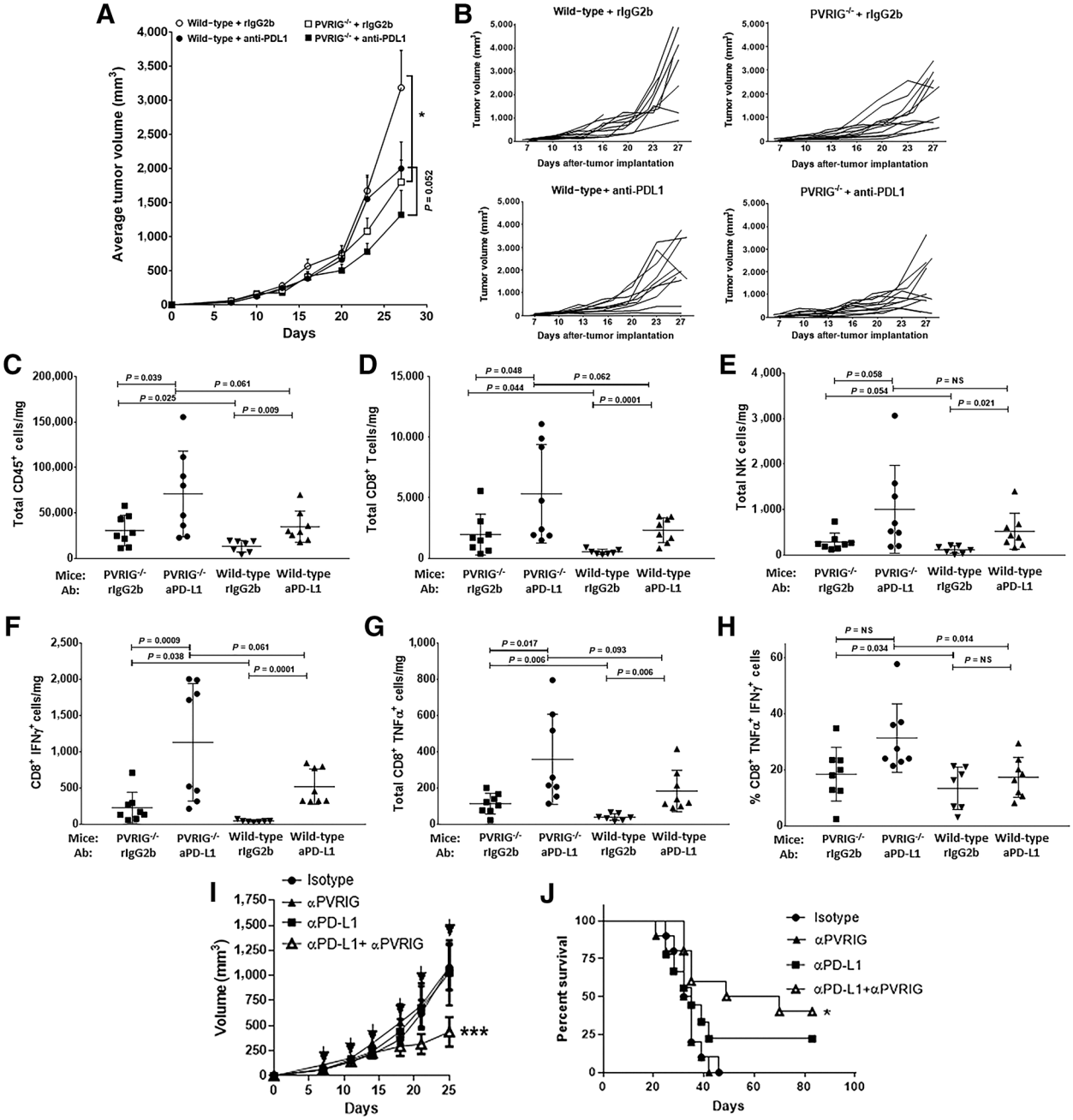

Figure 6.

PD-L1 blockade synergistically inhibits tumor growth in PVRIG-deficient mice or in combination with antagonistic anti-PVRIG antibodies. **A**, C57BL/6 wild-type or PVRIG$^{-/-}$ mice were subcutaneously injected with 5×10^5 MC38 cells. Beginning day 14, animals were treated with anti-PD-L1 or rat IgG2b isotype, twice weekly for 2 weeks. Tumor volumes were measured twice weekly. $n = 10$ mice per group; mean ± SEM is shown; *, $P < 0.05$ by an unpaired Student t test for wild-type mice versus PVRIG$^{-/-}$ mice, both treated with rat IgG2b isotype; $P = 0.052$ by an unpaired Student t test for wild-type mice versus PVRIG$^{-/-}$ mice, both treated with anti-PD-L1. **B**, Individual tumor growth curves are

shown. One representative experiment is shown ($n = 2$). **C–G**, In separate duplicate experiments, tumors were harvested on day 18 After mice had received 2 doses of anti-PD-L1 or isotype control. Dissociated tumors were enriched for $CD45^+$ cells prior to stimulation for 4 hours with PMA and ionomycin in the presence of brefeldin A. Graphs illustrate the total numbers per mg tumor tissue of (**C**) $CD45^+$ immune cells, (**D**) $CD8^+$ T cells, (**E**) $CD49b^+$ NK cells, (**F**) IFNγ-producing $CD8^+$ T cells, and (**G**) TNFα-producing $CD8^+$ T cells from isotype-treated as well as anti-PD-L1-treated wild-type and $PVRIG^{-/-}$ mice. **H**, Frequencies of $CD8^+$ $IFN\gamma^+$ $TNF\alpha^+$ effector cells in tumor-draining lymph nodes from anti-PD-L1/rIgG 2b isotype-treated $PVRIG^{-/-}$ and wild-type mice. For **C–H**, *P* values from an unpaired Student *t* test are shown. **I**, BALB/c mice were subcutaneously injected with 5×10^5 CT26 cells. On day 7 After inoculation, mice were treated with anti-PD-L1 and/or anti-PVRIG antibodies, twice weekly for 3 weeks (anti-PVRIG Ab treatment began on day 4; anti-PD-L1 Ab started on day 7). Tumor volumes (Ave ± SEM; $n = 10$ mice per group) are shown. ***, $P < 0.001$ (ANOVA) for anti-PD-L1 + rat IgG2b compared with anti-PD-L1 + anti-PVRIG-treated groups. **J**, Survival analysis. *, $P < 0.05$ (log-rank test) for anti-PD-L1 + rat IgG2b compared with anti-PD-L1 + anti-PVRIG-treated groups.